Biointerface Research in Applied Chemistry
Open-Access Journal (ISSN: 2069-5837)

Article
Volume 13, Issue 5, 2023, 440
https://doi.org/10.33263/BRIAC135.440

Structure-Based Rational Design and Virtual Screening of Valsartan Drug Analogs towards Developing Novel Inhibitors of Angiotensin II Type 1 Receptor

Hryhorii Y. Zahrychuk [1], Eugene S. Gladkov [2,3], Alexander V. Kyrychenko [2,3,*], Dmytro O. Poliovyi [1], Oksana M. Zahrychuk [1], Tetyana V. Kucher [1], Liliya S. Logoyda [1]

1 I. Horbachevsky Ternopil National Medical University, m.Voli, 1, Ternopil, 46001, Ukraine; zagrichuk@tdmu.edu.ua (H.Y.Z.); dpolov@tdmu.edu.ua (D.O.P.); zahrychuk.oks@tdmu.edu.ua (O.M.Z.); kucher_tv@tdmu.edu.ua (T.V.K.); logojda@tdmu.edu.ua (L.S.L.);
2 Institute of Chemistry, V. N. Karazin Kharkiv National University, 4 Svobody Sq., Kharkiv 61022, Ukraine; a.v.kyrychenko@karazin.ua (A.V.K.);
3 State Scientific Institution "Institute for Single Crystals", National Academy of Sciences of Ukraine, 60 Nauky Ave., Kharkiv 61072, Ukraine; eugenegladkov@gmail.com (E.S.G.);
* Correspondence: a.v.kyrychenko@karazin.ua (A.V.K.);

Scopus Author ID 6603879776
Received: 12.07.2022; Accepted: 28.08.2022; Published: 19.12.2022

Abstract: Antihypertensive sartans, such as valsartan (VST), have been proven to competitively block access to angiotensin II type 1 receptor (AT1R), regulating arterial blood pressure. Despite various commercially available sartan drugs, more effective novel inhibitors capable of appropriate blood pressure control are still required. Here we suggest the rational design of new valsartan analogs based on the structural modification of the parent VST drug molecule. Six transformation routes of a VST scaffold were considered. The first three schemes are based on functionalizing the VST carboxylic group either into an ester group or an amide moiety, following different degrees of further chemical modifications. Next, the role of tetrazole ring alkylation in tuning inhibitory activity is examined. Finally, two series of deep recursive structural alterations of a parent VST drug were also outlined utilizing Ugi and Passerini reactions. The inhibitory activity of all novel VST derivatives against AT1 receptor was screened using molecular docking calculations, followed by ADMET property analysis. Moreover, the binding affinity of ten well-known commercial sartans was also subject to re-docking against AT1R, allowing direct comparison with our designed VST derivatives. Altogether, our findings suggest that some proposed VST analogs may be promising candidates for developing and synthesizing novel antihypertensive agents.

Keywords: antihypertensive drug; angiotensin II type 1 receptor; valsartan; sartan; drug design; molecular docking.

© 2022 by the authors. This article is an open-access article distributed under the terms and conditions of the Creative Commons Attribution (CC BY) license (https://creativecommons.org/licenses/by/4.0/).

1. Introduction

Antagonists of Angiotensin II type 1 receptor (AT_1R) have been widely used to treat numerous diseases, such as hypertension, heart failure, myocardial infarction, and diabetic nephropathy [1]. Their beneficial effects are related to the inhibition of Angiotensin II by the blockade of AT_1R. Valsartan (VST) is an orally active antihypertensive drug that selectively inhibits AT_1R, causes a reduction in blood pressure, and is used to treat hypertension [2]. VST belongs to a broad family of antihypertensive sartans and has been well-tolerated in clinical

studies [3]. Therefore, it is a very good scaffold for generic industries and the development of novel, effective analogs. Moreover, many analytical methods have been developed to quantify and determine VST in biological fluids and pharmaceutical dosage forms [4-6].

Due to its essential pharmaceutical role, VST has also been explored by using computational chemistry tools. The conformational properties of VST have been analyzed both in solution and at the binding site of the receptor by using docking calculations and molecular dynamics (MD) simulations [7]. The interaction of valsartan and valsartan-Zn(II) complex with DNA has recently been studied by spectroscopic and *in silico* methods [8]. Most recently, active conformation of VST bound to AT_1R has been studied by all-atom MD simulations [9]. The binding interactions of the AT1 antagonist losartan with dipalmitoylphosphatidylcholine (DPPC) bilayer have been studied by MD simulations [10]. Molecular insights into the AT_1 antagonism based on biophysical and *in silico* studies of telmisartan have been reported [11]. The role of the AT_1 receptor flexibility in the binding of olmesartan and its derivatives in solution has been studied by all-atom MD simulations [12]. The role of the membrane bilayer in the recognition of candesartan by its G protein-coupled (GPC) AT_1 receptor has been explored [13]. Finally, interactions of valsartan with a sodium dodecyl sulfate (SDS) micelle have been examined by MD simulations [14].

Modifying the structural scaffold of drugs already available on the market is a common strategy used by the pharmaceutical industries to optimize a drug design's performance [15-18]. Following this strategy, here we suggest a rational drug design strategy based on the structural modification of the parent VST drug. We consider several transformation routes of a native VST scaffold to design novel VST analogs that reveal effective antihypertensive properties. Receptor-based molecular docking has become a powerful tool to screen the inhibitory activity of new compounds [18-28]. So, all designed VST derivatives were screened over molecular docking calculations against an AT_1 receptor. For hit candidates, the analysis of the drug-like property, such as Absorption, Distribution, Metabolism, Excretion, and Toxicity in the human body, referred to as ADMET, was evaluated. Finally, we also evaluated the binding affinity of ten well-known commercial sartans by their re-docking against AT_1R, which allows us to make a direct comparison with our suggested VST hit-analogs.

2. Materials and Methods

2.1. Molecular docking setup.

Molecular docking was carried out for all the designed valsartan derivatives against the angiotensin II type 1 receptor (AT_1R) (PDB ID: 4ZUD) [29]. The receptor and ligands were prepared with the AutoDock Tools (ADT) software, version 1.5.7 [30]. The hydrogen atoms were added to the PDB structure by the ADT software. The same software was used to calculate the Gasteiger charges at the receptor and ligands. All molecular docking calculations were carried out using the AutoDock Vina 1.1.2 software [31]. We performed the semi-flexible docking, so the receptor macromolecule was kept rigid, and the ligand molecules were conformationally flexible. The Lamarckian genetic algorithm was used as a research parameter. The size of the cubic box generated by ADT in the region of the AT_1 receptor interaction was assigned to be 60×60×60 Å, The center of the grid box was set at Cartesian coordinates x=-37.030, y=66.809 and z=26.261 with the grid point spacing set to 0.375 Å, respectively. For all molecular docking runs, the number of binding modes was set to 9 and the exhaustiveness to 200. We performed up to three independent runs for each ligand using different random seeds.

The best docking mode of the ligand corresponds to the largest ligand-binding affinity. Molecular graphics and visualization were performed using VMD 1.9.3 [32].

2.2. ADMET virtual screening.

The essential physicochemical characteristics of a bioactive molecule are its Absorption, Distribution, Metabolism, Excretion, and Toxicity in the human body, referred to as ADMET. In this study, we evaluated one of these parameters, namely, the lipophilicity parameter LogP, using the SwissADME web server [33].

3. Results and Discussion

3.1. Molecular model of AT_1R.

The AT_1R protein belongs to a family of G-protein coupled receptors (GPCRs) and consists of an amino-terminal extracellular region, a carboxyl group terminal intracellular tail, and eight, mostly hydrophobic, membrane-spanning α-helixes (TM1-TM8). Recently, several high-resolution structures of AT_1R and its complex with agonists have become available [29, 34]. Figure 1 shows the X-ray structure of AT_1R in complex with Olmesartan ligand (PDB 4ZUD). This high-resolution structure has already been used as the initial target for molecular docking and molecular dynamics simulations [35]. Therefore, after removing the ligand, we used this structure for our molecular docking calculations. Moreover, the binding position of the co-crystallized ligand allowed us to define a space grid box for molecular docking, as highlighted by a shaded area in Figure 1.

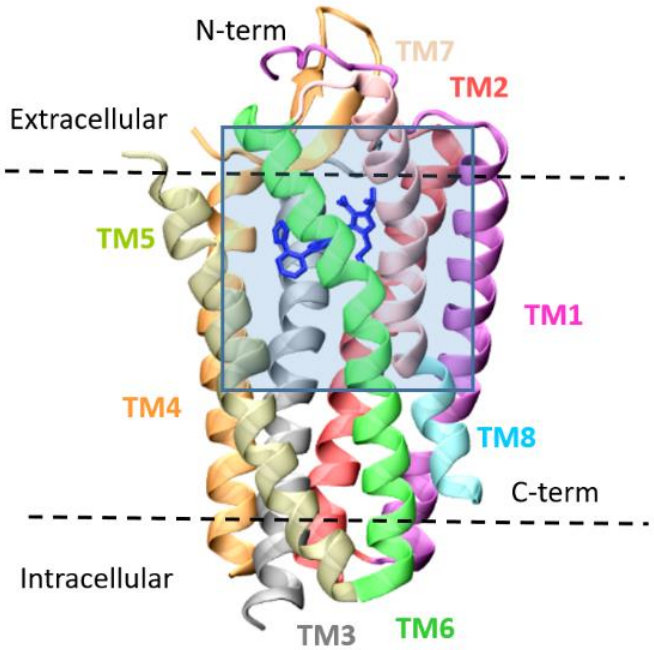

Figure 1. The X-ray structure of AT1R in complex with olmesartan is shown as a color-coded cartoon (PDB 4ZUD) [29]. Membrane boundaries, as defined by the CHARMM-GUI web server, are shown by dotted lines. Olmesartan is shown as licorice-colored blue. A grid box, selected for molecular docking calculations, is shown by a shaded square.

3.2. Rational design of new VST analogs.

The analysis of commercially available AT_1R antagonists revealed that they bear the following structural features [36]: (i) aromatic segments suitable to form π-π stacking

interactions, including biphenyl tetrazole or biphenyl carboxylate and various heterocyclic rings; (ii) acidic moieties as tetrazole or carboxylate groups that can be ionized and form various acid-base forms in solution; (iii) alkyl aliphatic chain responsible for its hydrophobic interactions with the active site of the AT_1R; (iv) other groups as hydroxyl or halogen that are also essential for specific interactions with the AT_1 receptor.

Therefore, a few series of new AT_1R inhibitors were designed based on six structural modification routes of a parent VST structure, as outlined in Scheme 1. In the first two series, either the NH moiety of the tetrazole heterocycle is alkylated, or the carboxylic group of VST is esterified. The proposed structural modifications lead to two series, **1a-s** and **2a-r**, which can easily be synthesized. We considered the introduction of bulk hydrophobic moieties to enhance the binding affinity of designed VST derivatives towards AT_1R. The list of proposed substituents R and R_1 and the physicochemical properties of compounds **1a-s** and **2a-r,** are summarized in Table 1.

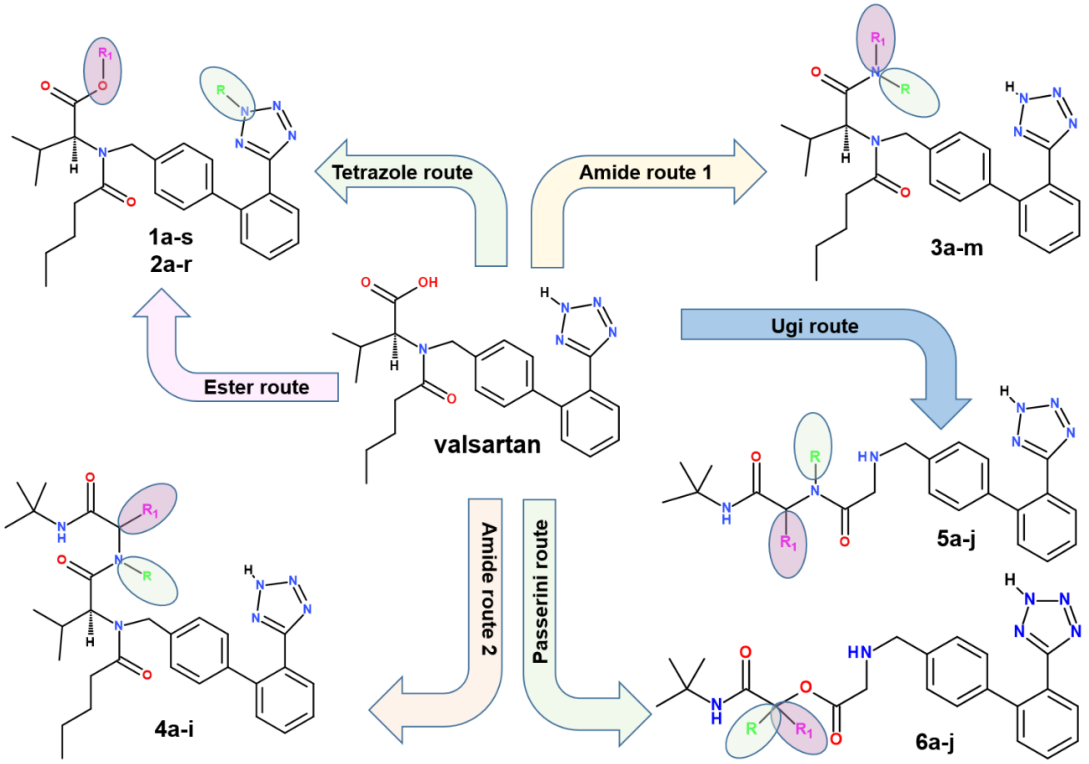

Scheme 1. Outline of structure-based design of some novel VST derivatives following six modification routes: the tetrazole ring alkylation (tetrazole route (**1a-s**)) and the carboxylic group esterification (ester route (**2a-r**)); two amide group routes with varying substituents R_1 (**3a-m**) and R (**4a-i**); Ugi and Passerini reaction routes lead to two other series of VST derivatives **5a-j** and **6a-j**.

Before in silico screening the inhibitory activity of newly designed VST derivatives, we first examined the activity of the parent VST drug 1a towards AT1R by molecular docking calculations. We found that docking calculations correctly reproduce VST binding into the active site of AT1R with the binding affinity of -8.5 kcal/mol (Table 1). Figure 2 shows the binding configurations of VST (1a) within the binding pocket of the AT1 receptor. The VST ligand makes close contact with Thr88 by the tetrazole ring. Other essential residues contributing to the ligand binding are Tyr35, Trp84, and Tyr87, respectively.

Theacid–base equilibria of VST are of great pharmacological importance because the action and liposolubility of VST depend on its charge, which, in turn, govern its passage across cell membranes during such processes as body absorption, distribution, and elimination. At physiological pH, VST can exist in anionic and dianionic forms [2, 6, 37].

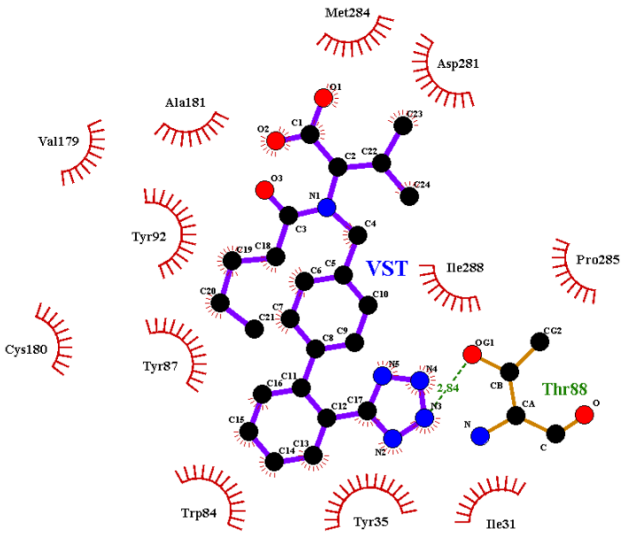

Figure 2. Molecular docking of VST(1a) to the crystal structure of AT1R (PDB ID: 4ZUD). The binding site of the ligand overlaps the AT1R binding pocket so that only the nearest residues surrounding VST are shown. Ligand is rendered in CPK mode; a hydrogen bond formed by Thr88 residue is indicated by a dotted line.

Table 1. Physicochemical parameters of designed VST derivatives **1a-s** and **2a-r**.

Ligand	R	R_1	Molecular formula	M_w (g/mol)	LogP[a]	E[b] (kcal/mol)
1a	H	H	$C_{24}H_{29}N_5O_3$	435.53	3.72	-8.5
1b	Methyl	H	$C_{25}H_{31}N_5O_3$	449.55	3.91	-8.5
1c	Ethyl	H	$C_{26}H_{33}N_5O_3$	463.57	4.24	-8.1
1d	Propyl	H	$C_{27}H_{35}N_5O_3$	477.60	4.53	-8.0
1e	*iso*-Propyl	H	$C_{27}H_{35}N_5O_3$	477.60	4.55	-8.3
1f	*n*-Butyl	H	$C_{28}H_{37}N_5O_3$	491.63	4.80	-8.2
1g	*tert*-Butyl	H	$C_{28}H_{37}N_5O_3$	491.63	4.75	-8.5
1h	Cyclobutyl	H	$C_{28}H_{35}N_5O_3$	489.61	4.63	-8.4
1i	Cyclopentyl	H	$C_{29}H_{37}N_5O_3$	503.64	4.87	-8.6
1j	Cyclohexyl	H	$C_{30}H_{39}N_5O_3$	517.66	5.26	-9.4
1k	Phenyl	H	$C_{30}H_{33}N_5O_3$	511.61	5.04	-9.3
1l	Benzyl	H	$C_{31}H_{35}N_5O_3$	525.64	5.06	-8.4
1m	4`-CF_3-C_6H_4	H	$C_{31}H_{32}N_5O_3F_3$	579.61	6.06	**-9.9**
1n	4`-CH_3-C_6H_4	H	$C_{31}H_{35}N_5O_3$	525.64	5.53	**-9.9**
1o	4`-F-C_6H_4	H	$C_{30}H_{32}N_5O_3F$	529.61	5.39	-9.6
1p	4`-HO-C_6H_4	H	$C_{30}H_{33}N_5O_4$	527.61	4.71	-9.1
1q	4`-CH_3O-C_6H_4	H	$C_{31}H_{35}N_5O_4$	541.64	5.18	-9.3
1r	4`-HOOC-C_6H_4	H	$C_{31}H_{33}N_5O_5$	555.62	4.64	-9.6
1s	4`-CH_3OOC- C_6H_4	H	$C_{32}H_{35}N_5O_5$	569.65	5.00	-9.5
2a	H	Methyl	$C_{25}H_{31}N_5O_3$	449.55	4.06	-8.2
2b	H	Ethyl	$C_{26}H_{33}N_5O_3$	463.57	4.35	-8.1
2c	H	Propyl	$C_{27}H_{35}N_5O_3$	477.60	4.73	-8.3
2d	H	*iso*-Propyl	$C_{27}H_{35}N_5O_3$	477.60	4.71	-8.7
2e	H	*n*-Butyl	$C_{28}H_{37}N_5O_3$	491.63	5.12	-8.0
2f	H	*tert*-Butyl	$C_{28}H_{37}N_5O_3$	491.63	4.88	-8.8
2g	H	Cyclobutyl	$C_{28}H_{35}N_5O_3$	489.61	4.80	-9.0
2h	H	Cyclopentyl	$C_{29}H_{37}N_5O_3$	503.64	5.06	-9.0
2i	H	Cyclohexyl	$C_{30}H_{39}N_5O_3$	517.66	5.41	-9.3
2j	H	Phenyl	$C_{30}H_{33}N_5O_3$	511.61	5.12	-9.1
2k	H	Benzyl	$C_{31}H_{35}N_5O_3$	525.64	5.28	-9.1
2l	H	4`-CF_3-C_6H_4	$C_{31}H_{32}N_5O_3F_3$	579.61	6.13	**-9.5**
2m	H	4`-CH_3-C_6H_4	$C_{31}H_{35}N_5O_3$	525.64	5.45	-9.2
2n	H	4`-F-C_6H_4	$C_{30}H_{32}N_5O_3F$	529.61	5.40	-9.3
2o	H	4`-HO-C_6H_4	$C_{30}H_{33}N_5O_4$	527.61	4.71	-9.2
2p	H	4`-CH_3O-C_6H_4	$C_{31}H_{35}N_5O_4$	541.64	5.20	-9.4
2q	H	4`-HOOC-C_6H_4	$C_{31}H_{33}N_5O_5$	555.62	4.82	-9.3
2r	H	4`-CH_3OOC- C_6H_4	$C_{32}H_{35}N_5O_5$	569.65	5.24	-9.2

a - LogP was estimated by the SwissADME web server (http://www.swissadme.ch).
b - The binding affinity was averaged after tree-independent docking runs.

For these reasons, we also docked the monoanion and dianion forms of VST and found that these forms have binding configurations very similar to that of neutral VST; however, their binding energy decreased from -8.2 to -8.3 kcal/mol. These findings suggest that VST prefers to bind into AT_1R in the neutral form. Therefore, we used the neutral VST scaffold for our further docking calculations.

To gain insight into the inhibitory activity of the new VST derivatives, their binding affinity towards AT_1R was explored and characterized using molecular docking calculations. We found that the compounds **1a-s** have a high binding affinity to AT_1R, so their docking binding scores varied in the range from -8.0 up to -9.9 kcal/mol, as summarized in Table 1. It could be noticed that the introduction of bulk-branched alkyl groups in **1c**-**1f** decreases the binding affinity compared to a parent VST drug. The highest affinity of -9.9 kcal/mol was observed for VST analogs **1m-1n** bearing 4`-$CF_3$-phenyl- or 4`-CH_3-phenyl-substituents.

It is instructive to highlight that the ester route derivatives **2a-r** revealed a moderate binding affinity (Table 1). Among this series, the best binding ligand **2l**, also bearing 4`-CF_3-phenyl-moiety, is only characterized by the binding energy of -9.5 kcal/mol. Therefore, we can suggest that the ester modification, while being easily synthetically affordable, has little potential for tuning the inhibitory activity of a parent VST drug.

Figure 3 shows the molecular docking for the best-binding analogs **1m** and **2l** to the AT_1 receptor. The binding site of both ligands overlaps the receptor binding pocket so that only the nearest residues surrounding the ligands are shown. Ligand **1m** binding is stabilized within the receptor pocket by strong H-bonding interactions with Thr87 and Thr260, as seen in Figure 3A. The other string polar interactions are between the ligand tetrazole ring and Arg167. In the case of **2l**, the binding interactions are very similar in many aspects to those of the parent VST drug. **2l** is bound at AT_1R mainly through the tetrazole-Thr88 interactions (Figure 3B).

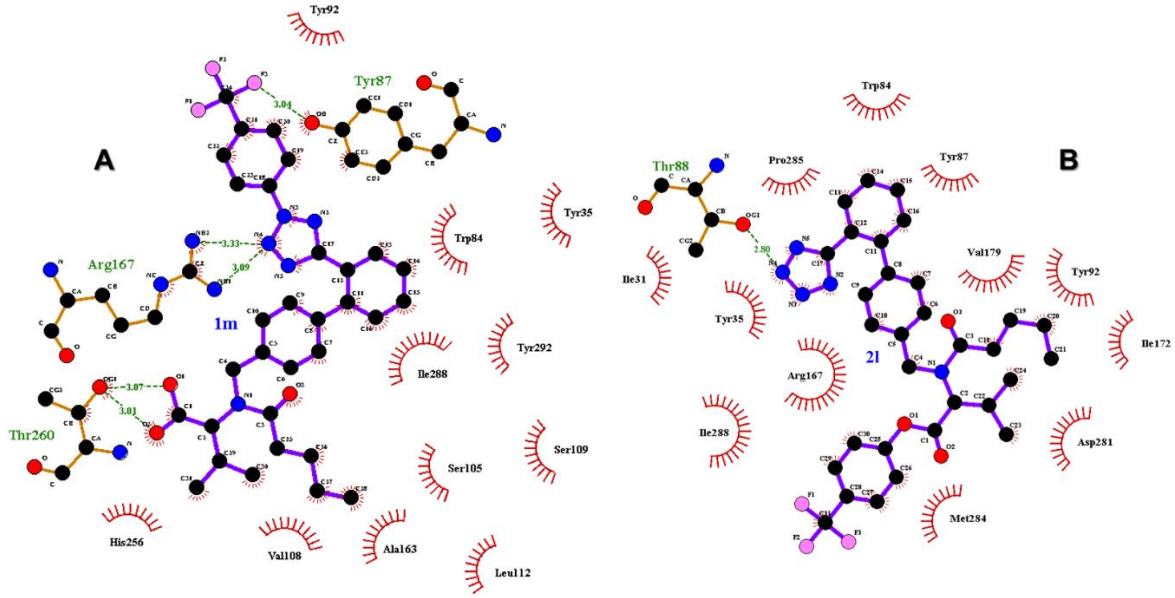

Figure 3. Molecular docking of the hit-ligands 1m and 2l to AT1R (PDB ID: 4ZUD). The ligands are rendered in CPK mode; dotted lines indicate the receptor residues involved in salt bridges and hydrogen bonds.

Next, we considered modifying the VST carboxylic group into an amide moiety with a different degree of complexity (Scheme 1). The list of proposed substituents R and R_1 for these two amide routes and the physicochemical properties of compounds **3a-m** and **4a-i** are summarized in Table 2.

Molecular docking calculations of amides **3a-m** revealed moderate binding affinity to AT_1R, so the best docking score ligand **3l**, bearing a benzyl moiety, is characterized by the binding energy of -9.7 kcal/mol, as summarized in Table 2. It should also be noted that the structural modification according to amide route 2 (Scheme 1) by introducing both methyl and bulky phenyl groups in **4h** has a similar effect on the binding score, which is found to be -9.8 kcal/mol.

Table 2. Physicochemical parameters and binding energy of VST derivatives **3a-m** and **4a-i** designed according to the two amide routes (Scheme 1).

Ligand	R	R_1	Molecular formula	Mw (g/mol)	LogP	E (kcal/mol)
3a	H	H	$C_{24}H_{30}N_6O_2$	434.53	3.39	-8.7
3b	H	Methyl	$C_{25}H_{32}N_6O_2$	448.56	3.70	-8.3
3c	H	Ethyl	$C_{26}H_{34}N_6O_2$	462.59	3.98	-8.5
3d	H	Propyl	$C_{27}H_{36}N_6O_2$	476.61	4.46	-8.6
3e	H	*iso*-Propyl	$C_{27}H_{36}N_6O_2$	476.61	4.35	-8.9
3f	H	*n*-Butyl	$C_{28}H_{38}N_6O_2$	490.64	4.66	-8.4
3g	H	*tert*-Butyl	$C_{28}H_{38}N_6O_2$	490.64	4.53	-8.9
3h	H	Cyclobutyl	$C_{28}H_{36}N_6O_2$	488.62	4.44	-9.0
3i	H	Cyclopentyl	$C_{29}H_{38}N_6O_2$	502.65	4.67	-9.3
3j	H	Cyclohexyl	$C_{30}H_{40}N_6O_2$	516.68	5.03	-9.8
3k	H	Phenyl	$C_{30}H_{34}N_6O_2$	510.63	4.76	-9.5
3l	H	Benzyl	$C_{31}H_{36}N_6O_2$	524.66	4.79	-9.7
3m	Methyl	Methyl	$C_{26}H_{34}N_6O_2$	462.59	3.90	-8.9
4a	H	H	$C_{30}H_{41}N_7O_3$	547.69	4.11	-9.2
4b	H	Methyl	$C_{31}H_{43}N_7O_3$	561.72	4.31	-9.2
4d	Methyl	H	$C_{31}H_{43}N_7O_3$	561.72	4.20	-9.3
4c	Methyl	Ethyl	$C_{33}H_{47}N_7O_3$	589.77	4.89	-9.4
4e	Methyl	Methyl	$C_{32}H_{45}N_7O_3$	575.74	4.46	-9.4
4f	Methyl	$2CH_3$	$C_{33}H_{47}N_7O_3$	589.77	4.58	-9.5
4g	Methyl	Phenyl	$C_{37}H_{47}N_7O_3$	637.81	5.38	-9.6
4h	Phenyl	Methyl	$C_{37}H_{47}N_7O_3$	637.81	5.48	-9.8
4i	Cyclopropyl	Methyl	$C_{34}H_{47}N_7O_3$	601.78	4.90	-9.2

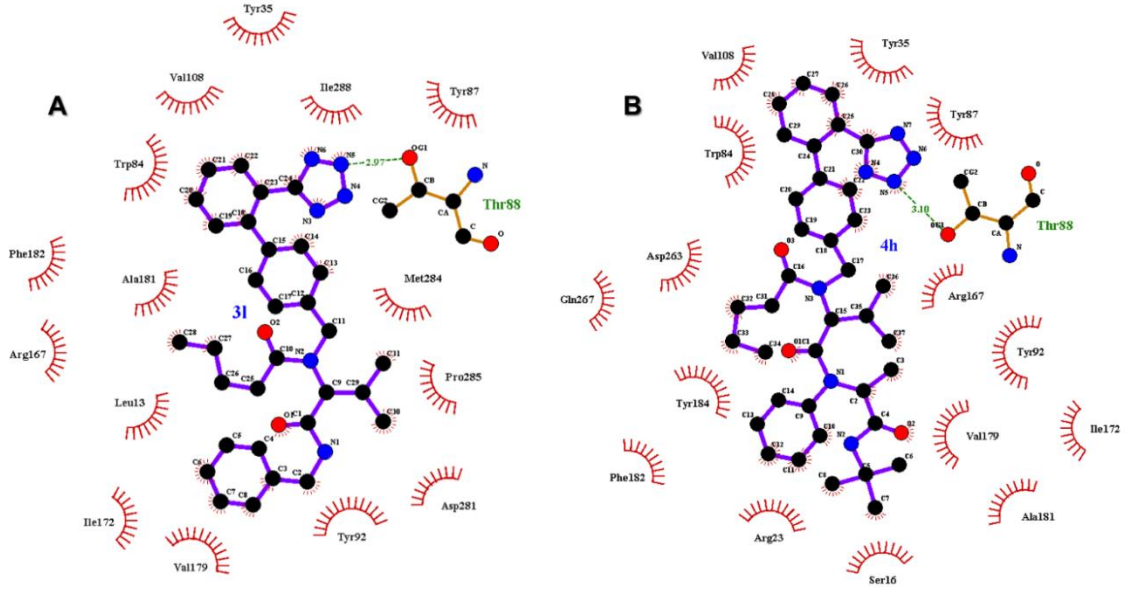

Figure 4. Molecular docking of the ligands **3l** (**A**) and **4h** (**B**) to AT_1R. The ligands are rendered in CPK mode; the receptor residues involved in salt bridges and hydrogen bonds are indicated by dotted lines.

Despite the structural modifications made in **3l** and **4h** analogs, the molecular docking suggest that their binding motif is conserved and resembles the main features of the binding interactions of the parent VST drug, as summarized in Figure 4. The tetrazole-Thr88 interactions mainly govern the binding of both ligands.

Some promising structure-based designs of VST analogs **1n**, **3l,** and **4h** have a better binding affinity towards AT_1R; however, their LogP parameter increases up to 4.8-6.1, which differs significantly from the VST value of 3.72 (Table 1). Therefore, two other structural modifications of the VTS drug were also considered.

The Ugi reaction is a multi-component reaction involving a ketone or aldehyde, an amine, an isocyanide, and a carboxylic acid [38]. Using the principles of combinatorial chemistry, the Ugi reaction could be utilized to synthesize VST analogs **5a-j** (Scheme 1).

We found that all designed analogs **5a-j** have a binding affinity to AT_1R higher than that of the parent VST drug, varying in a range of -9.4…-10.5 kcal/mol, as summarized in Table 3. The best binding analog **5d**, bearing a 4`-CF_3-phenyl-substituent, is characterized by the affinity of -10.5 kcal/mol, and logP equals 4.48. While the logP value of **5d** is found to be somewhat larger than that of VST, other analogs from this series, such as **5g**-**5h**, can compromise both these parameters and reveal the affinity of -10.2…-10.3 kcal/mol and logP of 2.59…3.72.

Table 3. Physicochemical parameters and binding energy for the VST derivatives designed according to the Ugi route (**5a-j**) and the Passerini route (**6a-j**) (Scheme 1).

Ligand	R	R_1	Molecular formula	Mw (g/mol)	LogP [a]	E [b] (kcal/mol)
5a	H	H	$C_{22}H_{27}N_7O_2$	421.50	2.12	-9.3
5b	*tert*-Butyl	H	$C_{26}H_{35}N_7O_2$	477.60	3.00	-9.6
5c	H	tert-Butyl	$C_{26}H_{35}N_7O_2$	477.60	3.12	-9.4
5d	4`-CF_3-C_6H_4	H	$C_{29}H_{30}N_7O_2F_3$	565.59	4.48	**-10.5**
5e	4`-CH_3OOC-C_6H_4	H	$C_{30}H_{33}N_7O_4$	555.63	3.39	-10.1
5f	4`-CH_3OOC-C_6H_4	Methyl	$C_{31}H_{35}N_7O_4$	569.65	3.78	-9.4
5g	4`-HOOC-C_6H_4	H	$C_{29}H_{31}N_7O_4$	541.60	2.59	-10.3
5h	4`-F-C_6H_4	H	$C_{28}H_{30}N_7O_2F$	515.58	3.72	-10.2
5i	4`-CH_3O-C_6H_4	H	$C_{29}H_{33}N_7O_3$	527.62	3.40	-10.2
5j	4`-HOOC-C_6H_4	Methyl	$C_{30}H_{33}N_7O_4$	555.63	2.89	-10.2
6a	H	H	$C_{22}H_{26}N_6O_3$	422.48	2.48	-8.8
6b	Methyl	H	$C_{23}H_{28}N_6O_3$	436.51	2.64	-9.1
6c	Methyl	Methyl	$C_{24}H_{30}N_6O_3$	450.53	3.01	-9.3
6d	*tert*-Butyl	H	$C_{26}H_{34}N_6O_3$	478.59	3.66	-9.1
6e	Phenyl	H	$C_{28}H_{30}N_6O_3$	498.58	3.65	-9.0
6f	4`-CF_3-C_6H_4	H	$C_{29}H_{29}N_6O_3F_3$	566.57	4.69	-9.7
6g	4`-CH_3OOC-C_6H_4	H	$C_{30}H_{32}N_6O_5$	556.61	3.68	-9.4
6h	4`-HOOC-C_6H_4	H	$C_{29}H_{30}N_6O_5$	542.59	2.80	-9.9
6i	4`-F-C_6H_4	H	$C_{28}H_{29}N_6O_3F$	516.57	3.91	-9.7
6j	4`-CH_3O-C_6H_4	H	$C_{29}H_{32}N_6O_4$	528.60	3.69	**-10.0**

The Passerini-type reaction involves an isocyanide, an aldehyde (or ketone), and a carboxylic acid to form an α-acyloxyamide [39]. This multi-component combinatorial chemistry reaction offers the opportunity to design VST analogs **6a-j** (Scheme 1).

All designed analogs **6a-j** were docked against AT_1R and demonstrated a high binding affinity, varying in a range of -8.8…-10.0 kcal/mol, as summarized in Table 3. The best analog **6j** bears a 4`-CH_3O-phenyl-substituent and is characterized by the binding affinity of -10.0 kcal/mol and logP of 3.69. Moreover, most analogs **6a-j**, except **6f**, all have promising AMDET parameters (Table 3). These analogs are characterized by M_w<500 kDa and logP in a range of 2.48-3.69, so they obey the Lippinsky rule (logP < 5.0).

Figure 5 summarizes the molecular docking calculations for the two hit-analogs **5d** and **6j**. It can be noticed that the strong binding of the ligand **5d** to the receptor is driven by multiple non-covalent interactions (Figure 5A). The binding mode of **5d** is changed compared to the parent VST drug, so the ligand is penetrated deeper into the receptor pocket. In the case of **6j**,

the strong polar interaction of the introduced –OCH_3 moiety with Arg167 is observed (Figure 5B). In addition, the receptor residue Tyr35 governs the other crucial interactions.

The recent crystal structure of the AT_1R in complex with an antagonist [18, 19] has shown that residues Arg167 in the second extracellular loop of the receptor and Val108 in TM3 interact with AT_1R antagonists [34, 40]. It is therefore believed that the molecular mechanism underlying AT_1R antagonism involves ligand interaction with these residues and stabilization of the tight hydrophobic network between TM3 and TM7, thus impeding the TM movements responsible for the increase in the distance between TM3 and TM7 during receptor activation [34]. These findings suggest that the ligand **6j** has a promising binding mode, which stabilizes the interaction network of TM3 with other TM segments via interactions with the bound ligand **6j**.

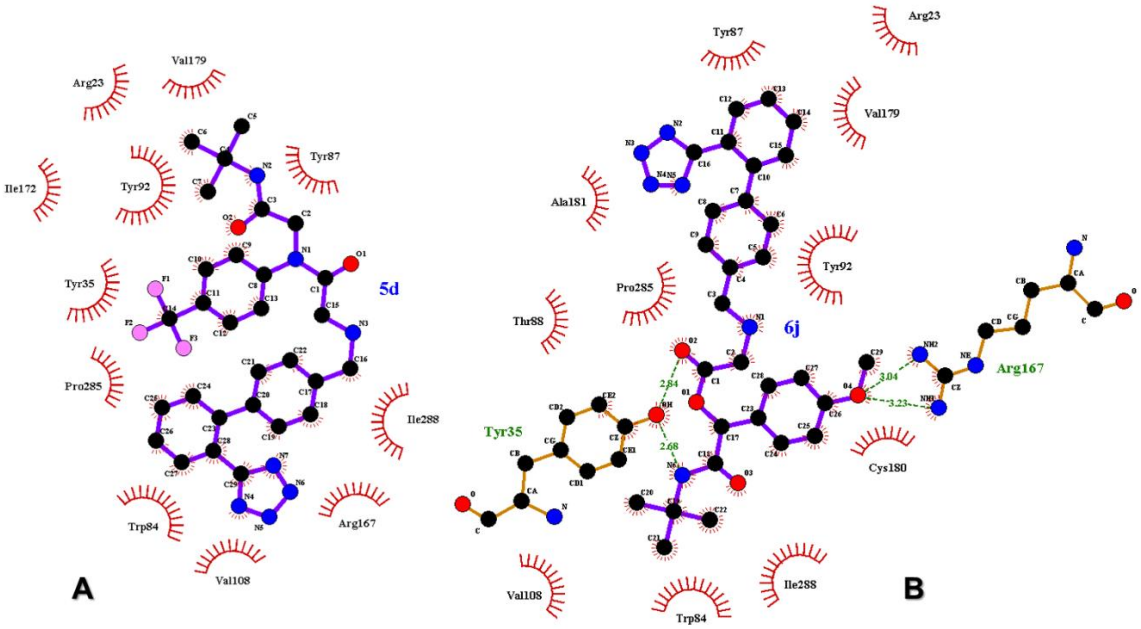

Figure 5. Molecular docking of the ligands **5d** (**A**) and **6j** (**B**) to AT_1R. The ligands are rendered in CPK mode; the receptor residues involved in salt bridges and hydrogen bonds are indicated by dotted lines.

3.3. Comparison with other sartans.

Sartans are nonpeptidergic AT_1R antagonists that have an essential role in the treatment of cardiovascular diseases. VST is one of the sartan family, among which other well-known analogs exist, such as forasartan, embusartan, candesartan, and losartan, and others [10, 41-42] that are in clinical trials or at preclinical stages of development (Scheme 2).

To compare the *in silico* predicted inhibitory action of our designed VST analogs with the available experimental activity, we carried out the docking calculations of ten known sartans, as summarized in Scheme 2 and Table 6. The results showed that most sartans showed stronger binding than the parent VST drug except losartan and eprosartan (Table 2). It can be noticed that one of the best-binding sartans is telmisartan, having a binding affinity of -10.8 kcal/mol. This affinity is the same order of magnitude as those of **5d** and **5g-5j** (Table 3), making them promising candidates for developing and synthesizing novel antihypertensive agents.

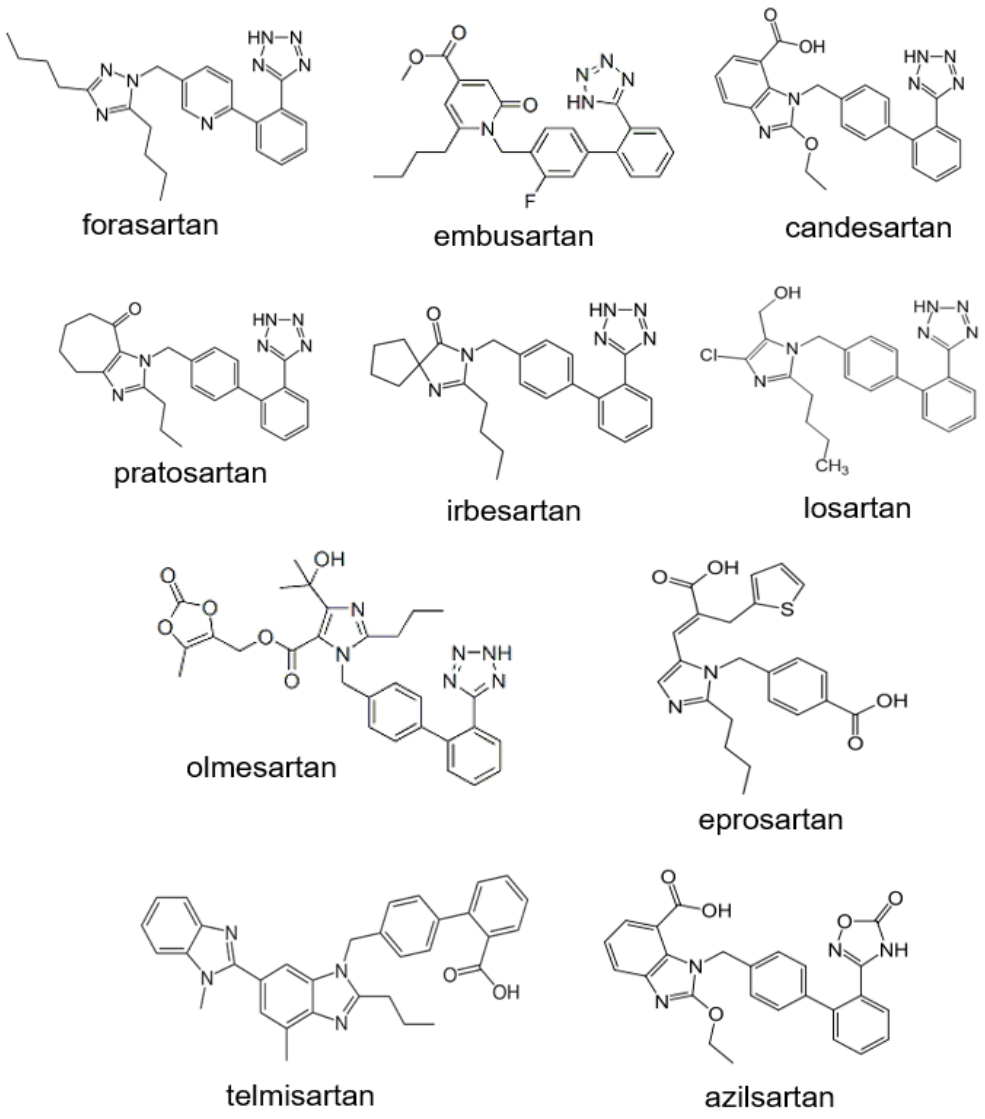

Scheme 2. Some known sartans.

Table 6. Comparison of physicochemical parameters and binding energy for valsartan and other sartans.

Compound	Molecular formula	Mw (g/mol)	Log P	E (kcal/mol)
valsartan	$C_{24}H_{29}N_5O_3$	435.53	3.72	-8.5
forasartan	$C_{23}H_{28}N_8$	416.52	4.14	-8.9
pratosartan	$C_{25}H_{26}N_6O$	426.51	4.06	-9.5
telmisartan	$C_{33}H_{30}N_4O_2$	514.62	5.92	-10.8
azilsartan	$C_{25}H_{20}N_4O_5$	456.45	3.79	-9.8
losartan	$C_{22}H_{23}N_6OCl$	422.91	3.86	-8.4
irbesartan	$C_{25}H_{28}N_6O$	428.53	4.28	-9.4
eprosartan	$C_{23}H_{24}N_2O_4S$	424.51	3.92	-8.0
embusartan	$C_{24}H_{29}N_5O_3$	435.53	3.72	-8.5
olmesartan	$C_{24}H_{26}N_6O_3$	446.50	3.08	-8.9
candesartan	$C_{24}H_{20}N_6O_3$	440.45	3.53	-9.5

4. Conclusions

The discovery of novel therapeutic candidates has always been associated with essential financial requirements and is also time-consuming; therefore, the application of computer-aided drug design has become a powerful technology in the drug discovery pipeline [43]. Here, the structure-guided rational design of new valsartan analogs has been performed. The analysis of known sartans revealed that they have some common essential structural features: (i) the

presence of aromatic segments, suitable to form π-π stacking interactions, including biphenyl tetrazole or biphenyl carboxylate and various heterocyclic rings; (ii) alkyl aliphatic linear or branched chain, responsible for its hydrophobic interactions with the active site of the AT_1R; (iv) other groups as hydroxyl or halogen that are also essential for specific interactions with the AT_1 receptor. Therefore, six different optimization modes of a parent VST scaffold have been considered. The first three schemes were based on functionalizing the VST carboxylic group into either an ester group or an amide moiety, following different degrees of further chemical modifications of these fragments. Next, tuning inhibitory activity by the tetrazole ring alkylation is examined. Finally, two series of deep recursive structural alterations of a parent VST drug were also outlined utilizing Ugi and Passerini reactions. The inhibitory activity of all novel VST derivatives against AT_1 receptor was screened using molecular docking calculations, followed by ADMET property analysis. Moreover, the binding affinity of ten well-known commercial sartans was also re-docked against AT_1R, allowing direct comparison with our designed VST derivatives. Altogether, our findings suggest that some proposed VST analogs, such as **5d** and **6j**, bearing 4`-$CF_3$-phenyl- or 4`-CH_3O-phenyl-moiety, may be promising pharmaceutical candidates for developing and synthesizing novel antihypertensive agents.

Funding

This research was funded for H.Y.Z., D.O.P., O.M.Z., and L.S.L by the Ministry of Health of Ukraine, Grant № 0120U104201.

Conflicts of Interest

The authors declare no conflict of interest.

References

1. Dasgupta, C.; Zhang, L. Angiotensin II receptors and drug discovery in cardiovascular disease. *Drug Disc. Today* **2011,** *16*, 22-34, https://doi.org/10.1016/j.drudis.2010.11.016.
2. Ardiana, F.; Suciati; Indrayanto, G. Valsartan. In Profiles of drug substances, excipients and related methodology, Brittain, H. G., Ed. Academic Press: **2015**, *40*, 431-493. https://doi.org/10.1016/bs.podrm.2015.01.004
3. Kantor, E. D.; Rehm, C. D.; Haas, J. S.; Chan, A. T.; Giovannucci, E. L. Trends in prescription drug use among adults in the united states from 1999-2012. *JAMA* **2015,** *314*, 1818-1830, https://doi.org/10.1001/jama.2015.13766.
4. Tran, T. T.-D.; Tran, P. H.-L.; Park, J.-B.; Lee, B.-J. Effects of solvents and crystallization conditions on the polymorphic behaviors and dissolution rates of valsartan. *Arch. Pharm. Res.* **2012,** *35*, 1223-1230, https://doi.org/10.1007/s12272-012-0713-7.
5. Skotnicki, M.; Gaweł, A.; Cebe, P.; Pyda, M. Thermal behavior and phase identification of valsartan by standard and temperature-modulated differential scanning calorimetry. *Drug Dev. Ind. Pharm.* **2013,** *39*, 1508-1514, https://doi.org/10.3109/03639045.2012.704379.
6. Muszalska, I.; Sobczak, A.; Dołhań, A.; Jelińska, A. Analysis of sartans: A review. *J. Pharm. Sci.* **2014,** *103*, 2-28, https://doi.org/10.1002/jps.23760.
7. Potamitis, C.; Zervou, M.; Katsiaras, V.; Zoumpoulakis, P.; Durdagi, S.; Papadopoulos, M. G.; Hayes, J. M.; Grdadolnik, S. G.; Kyrikou, I.; Argyropoulos, D.; Vatougia, G.; Mavromoustakos, T. Antihypertensive drug valsartan in solution and at the AT1 receptor: Conformational analysis, dynamic nmr spectroscopy, *in silico* docking, and molecular dynamics simulations. *J. Chem. Inf. Model.* **2009,** *49*, 726-739, https://doi.org/10.1021/ci800427s.

8. Kale, K. B.; Shinde, M. A.; Patil, R. H.; Ottoor, D. P. Exploring the interaction of valsartan and valsartan-Zn(II) complex with DNA by spectroscopic and in silico methods. *Spectrochim Acta A* **2022,** *264*, 120329, https://doi.org/10.1016/j.saa.2021.120329.
9. Wang, L.; Yan, F. Trans and cis conformations of the antihypertensive drug valsartan respectively lock the inactive and active-like states of angiotensin II type 1 receptor: A molecular dynamics study. *J. Chem. Inf. Model.* **2018,** *58*, 2123-2130, https://doi.org/10.1021/acs.jcim.8b00364.
10. Zervou, M.; Cournia, Z.; Potamitis, C.; Patargias, G.; Durdagi, S.; Grdadolnik, S. G.; Mavromoustakos, T. Insights into the molecular basis of action of the AT1 antagonist losartan using a combined NMR spectroscopy and computational approach. *Biochim. Biophys. Acta* **2014,** *1838*, 1031-1046, https://doi.org/10.1016/j.bbamem.2013.12.012.
11. Kritsi, E.; Potamitis, C.; Durdagi, S.; Zoumpoulakis, P.; Golic Grdadolnik, S.; Mavromoustakos, T. Molecular insights into the AT1 antagonism based on biophysical and in silico studies of telmisartan. *Med. Chem. Res.* **2013,** *22*, 4842-4857, https://doi.org/10.1007/s00044-012-0464-5.
12. Kellici, T. F.; Ntountaniotis, D.; Liapakis, G.; Tzakos, A. G.; Mavromoustakos, T. The dynamic properties of angiotensin II type 1 receptor inverse agonists in solution and in the receptor site. *Arabian J. Chem.* **2019,** *12*, 5062-5078, https://doi.org/10.1016/j.arabjc.2016.11.014.
13. Kiriakidi, S.; Chatzigiannis, C.; Papaemmanouil, C.; Tzakos, A. G.; Mavromoustakos, T. Exploring the role of the membrane bilayer in the recognition of candesartan by its GPCR AT1 receptor. *Biochimica et biophysica acta* **2020,** *1862*, 183142, https://doi.org/10.1016/j.bbamem.2019.183142.
14. Cao, C.; Mao, J.; Li, F.; Yang, M.; He, H.; Jiang, L.; Liu, M. Understanding the interaction between valsartan and detergents by NMR techniques and molecular dynamics simulation. *J. Phys. Chem. B* **2012,** *116*, 7470-7478, https://doi.org/10.1021/jp304304v.
15. Kellici, T. F.; Tzakos, A. G.; Mavromoustakos, T. Rational drug design and synthesis of molecules targeting the angiotensin II type 1 and type 2 receptors. *Molecules* **2015,** *20*, 3868-3897, https://doi.org/10.3390/molecules20033868.
16. Sabe, V. T.; Ntombela, T.; Jhamba, L. A.; Maguire, G. E. M.; Govender, T.; Naicker, T.; Kruger, H. G. Current trends in computer aided drug design and a highlight of drugs discovered via computational techniques: A review. *Europ. J. Med. Chem.* **2021,** *224*, 113705, https://doi.org/10.1016/j.ejmech.2021.113705.
17. Santana, K.; do Nascimento, L. D.; Lima e Lima, A.; Damasceno, V.; Nahum, C.; Braga, R. C.; Lameira, J. Applications of virtual screening in bioprospecting: Facts, shifts, and perspectives to explore the chemo-structural diversity of natural products. *Front. Chem.* **2021,** *9*, https://doi.org/10.3389/fchem.2021.662688.
18. Gurung, A. B.; Ali, M. A.; Lee, J.; Farah, M. A.; Al-Anazi, K. M. An updated review of computer-aided drug design and its application to COVID-19. *BioMed Res. Internat.* **2021,** *2021*, 8853056, https://doi.org/10.1155/2021/8853056.
19. Ajayeoba, T. A.; Woods, J. O.; Ayeni, A. O.; Ajayi, T. J.; Akeem, R. A.; Hosten, E. C.; Akinyele, O. F. Synthesis, crystallographic, computational and molecular docking studies of new acetophenone-benzoylhydrazones. *J. Mol. Struct.* **2021,** *1237*, 130275, https://doi.org/10.1016/j.molstruc.2021.130275.
20. Llanos, M. A.; Gantner, M. E.; Rodriguez, S.; Alberca, L. N.; Bellera, C. L.; Talevi, A.; Gavernet, L. Strengths and weaknesses of docking simulations in the SARS-CoV-2 era: The main protease (Mpro) case study. *J. Chem. Inf. Model.* **2021,** *61*, 3758-3770, https://doi.org/10.1021/acs.jcim.1c00404.
21. Zhang, S.; Krumberger, M.; Morris, M. A.; Parrocha, C. M. T.; Kreutzer, A. G.; Nowick, J. S. Structure-based drug design of an inhibitor of the SARS-CoV-2 (COVID-19) main protease using free software: A tutorial for students and scientists. *Eur. J. Med. Chem.* **2021,** *218*, 113390, https://doi.org/10.1016/j.ejmech.2021.113390.
22. Snizhko, A. D.; Kyrychenko, A. V.; Gladkov, E. S. Synthesis of novel derivatives of 5,6,7,8-tetrahydro-quinazolines using of α-aminoamidines and in silico screening of their biological activity. *Int. J. Mol. Sci.* **2022,** *23*, 3781, https://doi.org/10.3390/ijms23073781.
23. Luo, D.; Tong, J.-B.; Zhang, X.; Xiao, X.-C.; Bian, S. Computational strategies towards developing novel SARS-CoV-2 mpro inhibitors against COVID-19. *J. Mol. Struct.* **2022,** *1247*, 131378, https://doi.org/10.1016/j.molstruc.2021.131378.
24. Shcherbakov, D.; Baev, D.; Kalinin, M.; Dalinger, A.; Chirkova, V.; Belenkaya, S.; Khvostov, A.; Krut'ko, D.; Medved'ko, A.; Volosnikova, E.; Sharlaeva, E.; Shanshin, D.; Tolstikova, T.; Yarovaya, O.; Maksyutov, R.; Salakhutdinov, N.; Vatsadze, S. Design and evaluation of bispidine-based SARS-CoV-2 main protease inhibitors. *ACS Med. Chem. Lett.* **2021**, 140-147, https://doi.org/10.1021/acsmedchemlett.1c00299.
25. Mengist, H. M.; Dilnessa, T.; Jin, T. Structural basis of potential inhibitors targeting SARS-CoV-2 main protease. *Front. Chem.* **2021,** *9*, 622898, https://doi.org/10.3389/fchem.2021.622898.

26. Huynh, T.; Cornell, W.; Luan, B. *In silico* exploration of inhibitors for SARS-CoV-2's papain-like protease. *Front. Chem.* **2021,** *8*, 624163, https://doi.org/10.3389/fchem.2020.624163.
27. Hajbabaie, R.; Harper, M. T.; Rahman, T. Establishing an analogue based in silico pipeline in the pursuit of novel inhibitory scaffolds against the SARS coronavirus 2 papain-like protease. *Molecules* **2021,** *26*, 1134, https://doi.org/10.3390/molecules26041134.
28. Sadeghi, M.; Miroliaei, M. Inhibitory effects of selected isoquinoline alkaloids against main protease (M^{pro}) of SARS-CoV-2, in silico study. *In Silico Pharm.* **2022,** *10*, 5, https://doi.org/10.1007/s40203-022-00122-4.
29. Zhang, H.; Unal, H.; Desnoyer, R.; Han, G. W.; Patel, N.; Katritch, V.; Karnik, S. S.; Cherezov, V.; Stevens, R. C. Structural basis for ligand recognition and functional selectivity at angiotensin receptor. *J. Biol. Chem.* **2015,** *290*, 29127-29139, https://doi.org/10.1074/jbc.M115.689000.
30. Goodsell, D. S.; Morris, G. M.; Olson, A. J. Automated docking of flexible ligands: Applications of Autodock. *J. Mol. Recognit.* **1996,** *9*, 1-5, https://doi.org/10.1002/(SICI)1099-1352(199601)9:1<1::AID-JMR241>3.0.CO;2-6.
31. Trott, O.; Olson, A. J. Autodock Vina: Improving the speed and accuracy of docking with a new scoring function, efficient optimization, and multithreading. *J. Comput. Chem.* **2010,** *31*, 455-461, https://doi.org/10.1002/jcc.21334.
32. Humphrey, W.; Dalke, A.; Schulten, K. VMD: Visual molecular dynamics. *J. Mol. Graphics* **1996,** *14*, 33-38, https://doi.org/10.1016/0263-7855(96)00018-5.
33. Daina, A.; Michielin, O.; Zoete, V. Swissadme: A free web tool to evaluate pharmacokinetics, drug-likeness and medicinal chemistry friendliness of small molecules. *Sci. Rep.* **2017,** *7*, 42717, https://doi.org/10.1038/srep42717.
34. Zhang, H.; Unal, H.; Gati, C.; Han, Gye W.; Liu, W.; Zatsepin, Nadia A.; James, D.; Wang, D.; Nelson, G.; Weierstall, U.; Sawaya, Michael R.; Xu, Q.; Messerschmidt, M.; Williams, Garth J.; Boutet, S.; Yefanov, Oleksandr M.; White, Thomas A.; Wang, C.; Ishchenko, A.; Tirupula, Kalyan C.; Desnoyer, R.; Coe, J.; Conrad, Chelsie E.; Fromme, P.; Stevens, Raymond C.; Katritch, V.; Karnik, Sadashiva S.; Cherezov, V. Structure of the angiotensin receptor revealed by serial femtosecond crystallography. *Cell* **2015,** *161*, 833-844, https://doi.org/10.1016/j.cell.2015.04.011.
35. Anderson, S. D.; Tabassum, A.; Yeon, J. K.; Sharma, G.; Santos, P.; Soong, T. H.; Thu, Y. W.; Nies, I.; Kurita, T.; Chandler, A.; Alsamarah, A.; Kanassatega, R.-S.; Luo, Y. L.; Botello-Smith, W. M.; Andresen, B. T. *In silico* prediction of ARB resistance: A first step in creating personalized arb therapy. *PLoS Comput Biol* **2020,** *16*, e1007719, https://doi.org/10.1371/journal.pcbi.1007719.
36. Kellici, F. T.; Ntountaniotis, D.; Kritsi, E.; Zervou, M.; Zoumpoulakis, P.; Potamitis, C.; Durdagi, S.; Salmas, E. R.; Ergun, G.; Gokdemir, E.; Halabalaki, M.; Gerothanassis, P. I.; Liapakis, G.; Tzakos, A.; Mavromoustakos, T. Leveraging NMR and X-ray data of the free ligands to build better drugs targeting angiotensin II type 1 G-protein coupled receptor. *Curr. Med. Chem.* **2016,** *23*, 36-59, https://doi.org/10.2174/0929867323666151117122116.
37. Popović-Nikolić, M. R.; Popović, G. V.; Grujić, M.; Nikolić, K. M.; Agbaba, D. D. A theoretical study on ionization of sartans in aqueous media and on interactions with surfactant micelles. *J. Mol. Graph. Model.* **2018,** *82*, 67-73, https://doi.org/10.1016/j.jmgm.2018.04.008.
38. Dömling, A.; Ugi, I. Multicomponent reactions with isocyanides. *Angew. Chem., Int. Ed.* **2000,** *39*, 3168-3210, https://doi.org/10.1002/1521-3773(20000915)39:18<3168::AID-ANIE3168>3.0.CO;2-U.
39. Banfi, L.; Riva, R. The Passerini reaction. In *Organic reactions*, Wiley: **2005**, 1-140. https://doi.org/10.1002/0471264180.or065.01
40. Takezako, T.; Unal, H.; Karnik, S. S.; Node, K. Structure-function basis of attenuated inverse agonism of angiotensin II type 1 receptor blockers for active-state angiotensin II type 1 receptor. *Mol. Pharmacol.* **2015,** *88*, 488, https://doi.org/10.1124/mol.115.099176.
41. Bakheit, A. H. H.; Abd-Elgalil, A. A.; Mustafa, B.; Haque, A.; Wani, T. A. Telmisartan. Profiles of drug substances, excipients and related methodology, Brittain, H. G., Ed. Academic Press: **2015**, *40*, 371-429. https://doi.org/10.1016/bs.podrm.2015.01.003
42. Zakrocka, I.; Targowska-Duda, K. M.; Wnorowski, A.; Kocki, T.; Jóźwiak, K.; Turski, W. A. Angiotensin II type 1 receptor blockers inhibit Kat II activity in the brain — its possible clinical applications. *Neurotoxicity Res.* **2017,** *32*, 639-648, https://doi.org/10.1007/s12640-017-9781-2.
43. Adelusi, T. I.; Oyedele, A.-Q. K.; Boyenle, I. D.; Ogunlana, A. T.; Adeyemi, R. O.; Ukachi, C. D.; Idris, M. O.; Olaoba, O. T.; Adedotun, I. O.; Kolawole, O. E.; Xiaoxing, Y.; Abdul-Hammed, M. Molecular modeling in drug discovery. *Informatics Med. Unlocked* **2022,** *29*, 100880, https://doi.org/10.1016/j.imu.2022.100880.